Hybrid Integrator-Gain Systems: A Remedy for Overshoot Limitations in Linear Control?

S. J. A. M. van den Eijnden, M. F. Heertjes, *Member, IEEE*, W. P. M. H. Heemels, *Fellow, IEEE*, and H. Nijmeijer, *Fellow, IEEE*

***Abstract*—This letter shows that for a single-input single-output linear time-invariant plant having a real unstable open-loop pole, the overshoot inherent when using *any* stabilizing linear time-invariant feedback controller can be eliminated with a hybrid integrator-gain-based control strategy. Key design considerations underlying the presented controller are discussed, and an interpretation of the working mechanism is provided.**

***Index Terms*—HIGS, fundamental limitation, LTI control.**

I. Introduction

OVERSHOOT performance limitations inherent to linear time-invariant (LTI) feedback control [1], [2], motivate the use of so-called hybrid integrator-gain systems, further abbreviated as HIGS [3], [4]. To reduce overshoot, the main philosophy underlying HIGS is to keep the sign of the integrator's output the same as that of its input, thereby constantly forcing the system in the direction toward zero error. For achieving this, HIGS exploits a switching mechanism between a linear integrator and a gain, which is orchestrated according to algebraic conditions on HIGS' input-output pair. In turn, this results in a describing function which demonstrates a 20 dB/decade amplitude decay, similar to that of a linear integrator, but with an induced phase lag of only 38.15 degrees. These favourable characteristics are also found for reset elements [5], [6], [7], [8], [9]. The latter, however, make use of *discontinuous* control signals, whereas HIGS generates *continuous* (though non-smooth) signals, and thus is able to preserve a more concentrated power distribution in its output. As such, the relative contribution of higher-harmonics in the total output power is decreased. Especially in the context of high-precision mechatronic systems that have structural dynamics with weakly damped resonances, this provides a distinct advantage as it reduces the risk of exciting unwanted high-frequency dynamics in the plant.

Manuscript received March 17, 2020; revised May 20, 2020; accepted May 20, 2020. Date of publication June 1, 2020; date of current version June 12, 2020. Recommended by Senior Editor L. Menini. *(Corresponding author: S. J. A. M. van den Eijnden.)*

The authors are with the Department of Mechanical Engineering, Eindhoven University of Technology, 5600 MB Eindhoven, The Netherlands (e-mail: s.j.a.m.v.d.eijnden@tue.nl; m.f.heertjes@tue.nl; m.heemels@tue.nl; h.nijmeijer@tue.nl).

Digital Object Identifier 10.1109/LCSYS.2020.2998946

Although the performance-enhancing potential of HIGS-based control was already shown by the (experimental) results in [3], [4], and [10], an open question that remains is whether HIGS-based controllers can indeed go beyond performance achievable by LTI controllers. In this letter, one of the objectives is to answer this question positively. Hereto, HIGS is exploited in a feedback control configuration that aims at surpassing overshoot limitations of LTI control for single-input single-output (SISO) LTI plants. It is shown through a numerical example, that for a plant having a real unstable open-loop pole, the fundamental limitation that the closed-loop system necessarily exhibits overshoot in its step-response with *any* stabilizing LTI controller, is overcome with the proposed HIGS-based control strategy. The results are accompanied by key design considerations, which form important elements in a general philosophy for future control designs with HIGS.

It must be mentioned that other results are known in the literature that explicitly demonstrate the ability of specific nonlinear control strategies to truly go beyond performance obtained with LTI control. In [6], [11], examples are given of reset controllers that can meet certain transient performance specifications, which cannot be achieved with any LTI controller. Also, in [12] it is shown by a numerical example that overshoot requirements unattainable by any LTI controller can be met using phase-based variable-gain control. These examples, however, all employ discontinuous control.

The remainder of this letter is organized as follows. In Section II, a fundamental time-domain limitation of LTI systems linking the presence of a real unstable open-loop pole to the occurrence of overshoot is revisited, and HIGS is introduced. The HIGS-based controller is motivated in Section III, and through simulations it is shown that overshoot inherently present with any stabilizing LTI design, can be avoided with HIGS. Non-overshoot and parameter tuning are discussed in Section IV, and the main conclusions are given in Section V.

II. Preliminaries

A. A Fundamental Limitation of LTI Control

The results in this letter involve the class of SISO LTI feedback control systems, depicted in Fig. 1. Here, an LTI plant given by the transfer function $P(s)$, $s \in \mathbb{C}$, is placed in feedback interconnection with the LTI controller $C(s)$. The input to the plant consists of the control signal $u(t) \in \mathbb{R}$ at time

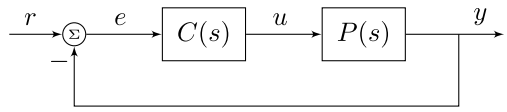

Fig. 1. Closed-loop system configuration with SISO LTI plant $P(s)$ and SISO LTI feedback controller $C(s)$.

$t \geq 0$. The plant output $y(t) \in \mathbb{R}$ is subtracted from the setpoint $r(t) \in \mathbb{R}$ to form the tracking error $e(t) := r(t) - y(t)$. In what follows, the setpoint r is assumed to be a unit-step, i.e., $r(t) = 1$ for $t \geq 0$, and $r(t) = 0$ otherwise.

In particular, a SISO LTI plant $P(s)$ having a real open-loop pole at $s = p$ with $p > 0$ is considered. When placing such a plant in feedback interconnection with *any* internally stabilizing LTI controller $C(s)$, a fundamental time-domain limitation exists between the rise-time and the amount of overshoot of the closed-loop system's step-response. Before explicitly stating this limitation, necessary definitions of internal stability, rise-time and overshoot are introduced.

Definition 1 [2]: Let the open-loop system in Fig. 1 be given by $L(s) = P(s)C(s)$. The closed-loop system is said to be internally stable if and only if the transfer function $S(s) = (1 + L(s))^{-1}$ has all of its poles in the open left half-plane, and there are no unstable pole-zero cancellations in $L(s)$.

Definition 2 [2]: The rise-time of a closed-loop system's step response y for zero initial conditions is defined as

$$t_r := \sup_{T>0} \left\{ T : y(t) \leq \frac{t}{T} \text{ for all } t \in [0, T] \right\}. \tag{1}$$

Definition 3 [2]: The overshoot of a closed-loop system's step response y for zero initial conditions is defined as

$$y_{os} := \sup_{t \geq 0} (-e(t)), \tag{2}$$

that is, the maximum value by which the step response exceeds the final setpoint value.

Proposition 1 [2]: Suppose that $P(s)$ has a real pole at $s = p$ with $p > 0$. If the closed-loop system is internally stabilized by any LTI controller $C(s)$, then the resulting step response y exhibits overshoot, which satisfies the lower-bound

$$y_{os} \geq \frac{(pt_r - 1)\exp(pt_r) + 1}{pt_r} \geq \frac{pt_r}{2}. \tag{3}$$

Proof: The proof can be found in [2, Sec. 1.3]. ■

B. Hybrid Integrator-Gain System (HIGS)

The hybrid integrator-gain system (HIGS) is formulated as the discontinuous piecewise-linear (PWL) system

$$\mathcal{H} : \begin{cases} \dot{x}_h = \omega_h z & \text{if } (z, u_h, \dot{z}) \in \mathcal{F}_1, \\ x_h = z & \text{if } (z, u_h, \dot{z}) \in \mathcal{F}_2, \\ u_h = x_h, \end{cases} \tag{4}$$

in which $x_h(t) \in \mathbb{R}$ denotes the state of the integrator, $z(t) \in \mathbb{R}$ is the input to HIGS at time $t \geq 0$, where z is assumed to be continuously differentiable, $\dot{z}(t) \in \mathbb{R}$ is the corresponding time-derivative, and $u_h(t) \in \mathbb{R}$ is the generated output at time $t \geq 0$. The design parameter $\omega_h \in (0, \infty)$ is the integrator frequency. The sets $\mathcal{F}_1$ and $\mathcal{F}_2$ denote subregions of $\mathbb{R}^3$ in which HIGS represents (i) an integrator or (ii) a gain. By design, the union of these sets is given by

$$\mathcal{F} := \mathcal{F}_1 \cup \mathcal{F}_2 = \left\{ (z, u_h, \dot{z}) \in \mathbb{R}^3 \mid z u_h \geq u_h^2 \right\}, \tag{5}$$

which describes the $[0, 1]$-sector. As motivated in [3], [13], HIGS is intended to primarily exhibit integrator dynamics. Therefore, the region $\mathcal{F}_1$ is selected maximal in the sense that a switch from 'integrator-mode' to 'gain-mode' is invoked only when the $(z, u_h, \dot{z})$-trajectory tends to leave the sector $\mathcal{F}$ when following the integrator dynamics. A switch to gain-mode, dictated by the set $\mathcal{F}_2$, prevents the trajectory from leaving the sector $\mathcal{F}$ by forcing it to move along the sector boundary $u_h = z$. The sets governing the active dynamics of HIGS are given by

$$\mathcal{F}_1 := \mathcal{F} \setminus \mathcal{F}_2, \tag{6a}$$

$$\mathcal{F}_2 := \left\{ (z, u_h, \dot{z}) \in \mathcal{F} \mid u_h = z \wedge \omega_h z^2 > \dot{z} z \right\}. \tag{6b}$$

A visualization of these sets can be found in [3, Sec. 2]. It is assumed that $x_h(0) \in \mathcal{F}$ to guarantee $x_h(t) \in \mathcal{F}$ for all $t \geq 0$. For a formal introduction of HIGS, inspired by projected dynamical systems, along with a proof for global existence of solutions, the reader is referred to [13]. Specific control applications with HIGS can be found in [3], [4], [10].

III. Overcoming Overshoot Limitations With HIGS

In this section, the HIGS-based control strategy is presented, and by a numerical case study it is shown that the overshoot-performance limitation stated in Proposition 1 can be overcome with this approach. In order to motivate the strategy, first an LTI controller example is considered.

A. LTI Control Example

Consider the LTI plant

$$P(s) = \frac{(s + q)\omega^2}{(s - p)(s^2 + 2\zeta\omega s + \omega^2)}, \tag{7}$$

which has a real unstable pole at $s = p$, with $p = 1$, two stable poles at $s = -\omega(\zeta \pm \sqrt{\zeta^2 - 1})$, where $\omega = 5 \cdot 2\pi$ rad/s and $\zeta = 1.5$, and a zero at $s = -q$ with $q = 3$. As a control objective, a feedback controller $C(s)$ must be designed that (i) *internally stabilizes* the closed-loop system, and (ii) achieves a *zero steady-state tracking error* when the closed-loop system is subject to a unit-step reference input r. The requirement for internal stability removes the possibility for $C(s)$ to introduce an unstable pole-zero cancellation, whereas the latter objective necessitates integral action in the controller $C(s)$ by virtue of the internal model principle (see [15]). A controller $C(s)$ suitable for this purpose is designed on the basis of the Nyquist stability criterion [17, Sec. 6.3], resulting in

$$C(s) = k_p \cdot \frac{\omega_i}{s}, \tag{8}$$

with proportional gain $k_p = 10$ N/m, and integrator frequency $\omega_i = 1$ rad/s. Note that for achieving the given control objectives, other types of LTI controllers can be considered as well (although all would result in overshoot by virtue of Proposition 1). To keep the exposition simple and preserve insights in the effects of the controller on overshoot, the choice for an integrator in (8) is made.

According to Proposition 1, the closed-loop system (7), (8) must exhibit overshoot in its step-response. In this specific example, an aspect that additionally contributes to the presence of overshoot is the necessity for integral control. This is understood as follows. As initially the error $e(t) > 0$, the integrator in (8) 'sums' the error over time to provide a positive input $u(t) > 0$ for driving the system toward the setpoint. For achieving zero steady-state error, it follows from the final value theorem (see [14]) that

$$\lim_{t\to\infty} u(t) = \lim_{s\to 0} \frac{sC(s)}{1 + C(s)P(s)} \cdot \frac{1}{s} = -\frac{p}{q} < 0. \tag{9}$$

Hence, a negative steady-state input is needed for zero steady-state error. This implies a sign change of u, which is only achieved if e changes sign, thus causing overshoot.

B. HIGS-Based Control Example

Given the previous observations, a HIGS-based integrator is proposed that adopts the functionality of a linear integrator for achieving zero steady-state error, but aims at reducing/eliminating overshoot, and simultaneously stabilizes the closed-loop system. The strategy is depicted in Fig. 2, where $C_1(s)$, and $C_2(s)$ are LTI filters specifically chosen as

$$C_1(s) = k_p\left(\frac{s}{\omega_c} + 1\right) \text{ and } C_2(s) = \frac{\omega_i}{s}, \tag{10}$$

with $\omega_c = \omega_h \cdot |1 + 4j/\pi|$. The particular choice for the filters in (10) and parameter ω_c is based on the following quasi-linear reasoning. The describing function of HIGS, i.e., the complex mapping from a sinusoidal input $z(t) = \sin(\omega t)$ to the first harmonic in $u_h(t)$, is given by

$$D(j\omega) = \frac{\omega_h}{j\omega}\left(\frac{\gamma}{\pi} + j\frac{e^{-2j\gamma} - 1}{2\pi} - 4j\frac{e^{-j\gamma} - 1}{2\pi}\right) + \left(\frac{\pi - \gamma}{\pi} + j\frac{e^{-2j\gamma} - 1}{2\pi}\right), \tag{11}$$

where $\gamma = 2\arctan(\omega/\omega_h) \in [0, \pi]$ denotes the (periodic) switching instant. Explicit derivation of the describing function (11) can be found in [4, Sec. 2.1]. Evaluating (11) reveals first-order low-pass magnitude characteristics with cross-over frequency at $\omega_c = \omega_h \cdot |1 + 4j/\pi|$ rad/s, accompanied by a phase lag that does not exceed 38.15 degrees, see Fig. 3 (gray curve). The filter $C_1(s)$ 'compensates' the magnitude characteristics, and provides additional phase lead. As a result of this, the describing function of the HIGS-based integrator, given by

$$I(j\omega) = C_1(j\omega)D(j\omega)C_2(j\omega), \tag{12}$$

admits magnitude characteristics similar to the linear integrator in (8), but with locally reduced phase lag. This is shown in Fig. 3 by the black curve. The apparent phase advantage hints toward the possibility for improving overshoot properties.

From a quasi-linear perspective, the particular ordering of the filters in the HIGS-based integrator is interchangeable. From a time-domain performance perspective, however, this is not the case as the switching behaviour of HIGS is directly determined by its input z, and, therefore, by the choice for the filter $C_1(s)$. The rationale behind the proposed configuration in Fig. 2 for potentially achieving non-overshoot performance can be explained as follows.

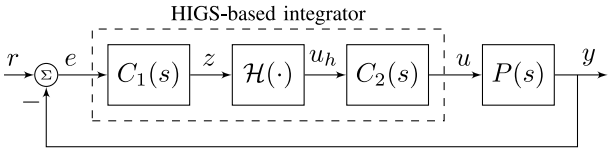

Fig. 2. Closed-loop system with HIGS-based integrator.

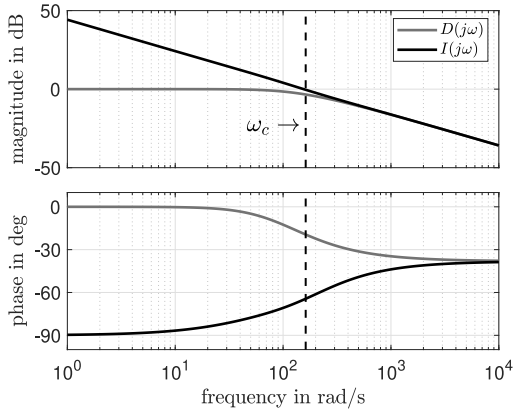

Fig. 3. Describing function $D(j\omega)$ (grey) and $I(j\omega)$ (black).

- By using the output of HIGS directly as an input to the linear integrator in the HIGS-based controller, a control mode-switching mechanism is provided for filling and depletion of the linear integrator buffer at a variable rate, hence, $C_2(s)$ is located directly after HIGS. Note that, despite the integrator-mode, HIGS cannot maintain a buffer necessary for achieving zero steady-state error due to its sector-boundedness, underlining the necessity for including a pure integrator in the design.
- Due to the previous choice, the output of HIGS should admit zero-crossings for allowing a sign-change of the linear integrator's output, see also the discussion at the end of Section III-A. Sign-equivalence of the HIGS' input and output signal then necessitates the input of HIGS to admit zero-crossings. For achieving non-overshoot performance, by definition, a sign-change of e must be avoided. Hence, e cannot be used directly as an input to HIGS. Rather, $C_1(s)$ as in (10) is used for realizing a filtered version of e, i.e., $z = k_p(\frac{\dot{e}}{\omega_c} + e)$. The weighted combination of e and $\dot{e}$ creates the possibility for z to have zero-crossings without e crossing zero.

Remark 1: For a practical implementation of the HIGS-based controller, in particular the non-proper filter $C_1(s)$ in (10), the following adaptation is proposed: $\hat{C}_1(s) = C_1(s)F(s)$, and $\hat{C}_2(s) = C_2(s)F^{-1}(s)$, where $F(s) = \frac{1}{\tau s+1}$ and $\tau > 0$ is chosen sufficiently small. The filters $\hat{C}_1$, $\hat{C}_2$ are proper filters. Note that the describing function characteristics in (12) remain unchanged by these transformations.

The step-response of the plant (7) in feedback with the HIGS-based controller, the latter being the series interconnection of the filters $\hat{C}_1(s)$, and $\hat{C}_2(s)$ with $\tau = 5 \cdot 10^{-3}$ see Remark 1, and the HIGS in (4) with $\omega_h = 0.8$ rad/s, is shown in Fig. 4 (in red), along with the generated control output u. The step-response and control output with the linear controller (8) are shown in black. Overshoot is

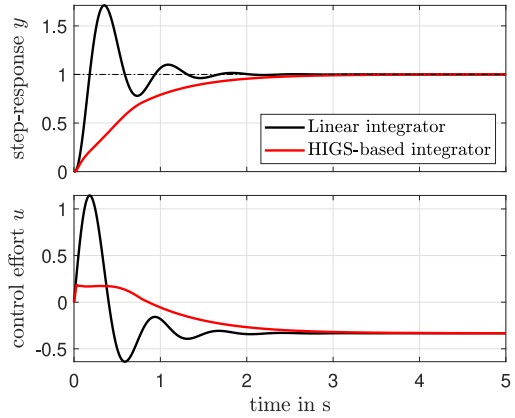

Fig. 4. Step-response y (top) and control output u (bottom) of the linear (black) and nonlinear (red) closed-loop system.

clearly present for the linear system, whereas for the HIGS-based control system there is no overshoot at all, under fairly limited control effort. It is emphasized that for the linear control system, the overshoot in Fig. 4 can be reduced by considering different LTI filters, e.g., PID-filters, but cannot be avoided as a consequence of the fundamental limitation stated in Proposition 1. Moreover, given the rise-time $t_r = 0.83$ s of the HIGS-controlled system, any linear controller resulting in a similar rise-time yields an overshoot of at least $y_{os} = 0.415$ according to the lower-bound in (3). These observations highlight the distinct advantage of the HIGS-based controller over any LTI controller in achieving improved (non-)overshoot performance.

It remains to show for this example that the HIGS-based integrator stabilizes the closed-loop system, and thus truly overcomes the fundamental limitation stated in Proposition 1. In this context, the notion of input-to-state stability (ISS) [16, Definition 2.1] is adopted, as it links to the concept of internal stability given in Definition 1. Consider the closed-loop system formulation

$$\Sigma: \begin{cases} \dot{x} = A_i x + B_i w, & \text{if } q \in \mathcal{F}_i, \quad i = \{1, 2\}, \\ q = Cx + Dw, \end{cases} \tag{13}$$

where $x = [x_p, x_i, x_h, x_f]^\top \in \mathbb{R}^6$ augments the states of $P(s)$, $\hat{C}_2(s)$, HIGS, and $\hat{C}_1(s)$, respectively, $w \in \mathbb{R}^n$ is the vector of exogenous input signals, and $q = [z, u_h, \dot{z}]^\top$ are the signals that determine mode-switching of HIGS. The corresponding system matrices are provided in the Appendix.

For verifying ISS of the closed-loop system in (13), it is sufficient to find a matrix $P = P^\top \succ 0$ and a vector $\Theta \in \mathbb{R}^6$ that satisfy the linear matrix inequalities (LMIs)

$$A_1^\top P + P A_1 \prec 0, \tag{14a}$$
$$A_2^\top P + P A_2 + \Pi^\top \Theta + \Theta^\top \Pi \prec 0, \tag{14b}$$

with $\Pi = \begin{bmatrix} 1 & -1 & 0 \end{bmatrix} C$. When feasible, the LMIs in (14) guarantee the existence of a common quadratic Lyapunov function $V(x) := x^\top P x$ for the system (13) with $w = 0$. To see this, observe that $P \succ 0$ implies V to be positive definite. Furthermore, (14a) implies that V is strictly decreasing along the trajectories of the system in integrator-mode. Since $\mathcal{F}_2 \subseteq \ker \Pi$, it follows from Finsler's lemma that (14b) implies a strict decrease of V in gain-mode. As such, V classifies as a suitable Lyapunov function for the system. Next, since w is an affine input to (13), similar arguments as in [18, Ch. 4, Sec. 4.9] can be employed to show that V classifies as an ISS-Lyapunov function [16, Definition 2.2], proving ISS of the closed-loop system (13) with respect to all bounded inputs w. The LMI conditions (14) are solved numerically, and the resulting matrix P and vector Θ are given in the Appendix.

Given feasibility of the LMIs in (14), together with the absence of overshoot in the closed-loop system's step response as observed from Fig. 4, it is concluded that the fundamental limitation presented in Proposition 1 is overcome with the proposed HIGS-based control strategy for the example discussed.

IV. Non-Overshoot and Parameter Tuning

For better understanding the mechanism resulting in the absence of overshoot in Fig. 4, and obtaining further directions for controller design and parameter tuning, consider the trajectories depicted in Fig. 5. First, remark from Fig. 5(a)

$$\left[A_1 | B_1\right] = \left[\begin{array}{cccccc|cc} 0 & 1 & 0 & 0 & 0 & 0 & 0 & 0 \\ 0 & 0 & 1 & 0 & 0 & 0 & 0 & 0 \\ p\omega^2 & 2p\zeta\omega - \omega^2 & p - 2\zeta\omega & \omega^2 & \tau\omega^2\omega_i & 0 & 0 & 0 \\ 0 & 0 & 0 & 0 & \omega_i & 0 & 0 & 0 \\ -\frac{k_p\omega_h q}{\tau\omega_c} & \frac{-k_p\omega_h}{\tau\omega_c} & 0 & 0 & 0 & k_p\omega_h\left(\frac{\tau\omega_c - 1}{\tau\omega_c}\right) & \frac{\omega_h}{\tau\omega_c} & 0 \\ -\frac{q}{\tau} & -\frac{1}{\tau} & 0 & 0 & 0 & -\frac{1}{\tau} & \frac{1}{\tau} & 0 \end{array}\right] \tag{15}$$

$$\left[A_2 | B_2\right] = \left[\begin{array}{cccccc|cc} 0 & 1 & 0 & 0 & 0 & 0 & 0 & 0 \\ 0 & 0 & 1 & 0 & 0 & 0 & 0 & 0 \\ p\omega^2 & 2p\zeta\omega - \omega^2 & p - 2\zeta\omega & \omega^2 & \tau\omega^2\omega_i & 0 & 0 & 0 \\ 0 & 0 & 0 & 0 & \omega_i & 0 & 0 & 0 \\ \frac{k_p q}{\tau}\left(\frac{1-\tau\omega_c}{\tau\omega_c}\right) & \frac{k_p}{\tau}\left(\frac{1-q\tau}{\tau\omega_c} - 1\right) & -\frac{k_p}{\tau\omega_c} & 0 & 0 & \frac{k_p}{\tau}\left(\frac{1-\tau\omega_c}{\tau\omega_c}\right) & \frac{k_p}{\tau}\left(\frac{\tau\omega_c - 1}{\tau\omega_c}\right) & \frac{k_p}{\tau\omega_c} \\ -\frac{q}{\tau} & -\frac{1}{\tau} & 0 & 0 & 0 & -\frac{1}{\tau} & \frac{1}{\tau} & 0 \end{array}\right] \tag{16}$$

$$\left[C | D\right] = \left[\begin{array}{cccccc|cc} -\frac{k_p q}{\tau\omega_c} & \frac{k_p}{\tau\omega_c} & 0 & 0 & 0 & k_p\left(\frac{\tau\omega_c - 1}{\tau\omega_c}\right) & \frac{k_p}{\tau\omega_c} & 0 \\ 0 & 0 & 0 & 0 & 1 & 0 & 0 & 0 \\ \frac{k_p q}{\tau}\left(\frac{1-\tau\omega_c}{\tau\omega_c}\right) & \frac{k_p}{\tau}\left(\frac{1-q\tau}{\tau\omega_c} - 1\right) & -\frac{k_p}{\tau\omega_c} & 0 & 0 & \frac{k_p}{\tau}\left(\frac{1-\tau\omega_c}{\tau\omega_c}\right) & \frac{k_p}{\tau}\left(\frac{\tau\omega_c - 1}{\tau\omega_c}\right) & \frac{k_p}{\tau\omega_c} \end{array}\right] \tag{17}$$

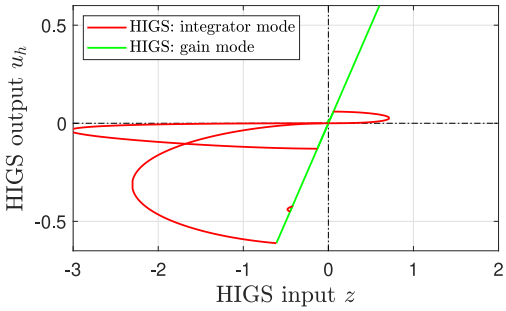

(a) HIGS input z versus HIGS output u_h.

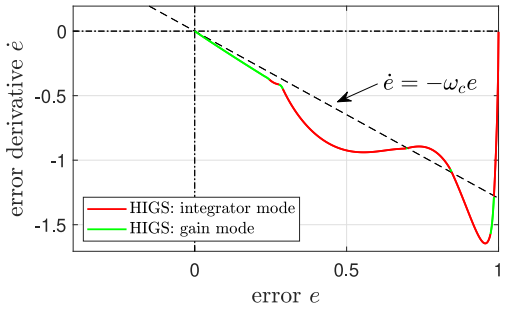

(b) Error e versus error derivative $\dot{e}$ with $\omega_h = 0.8$ rad/s.

Fig. 5. Trajectories of the HIGS-controlled system.

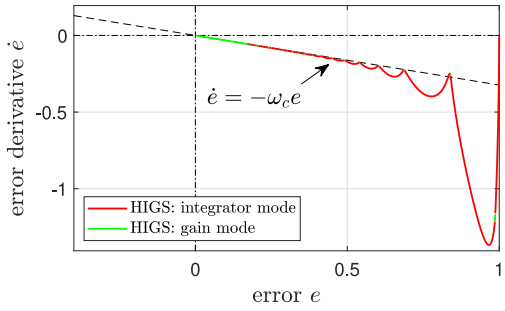

(a) Error e versus error derivative $\dot{e}$ with $\omega_h = 0.2$ rad/s.

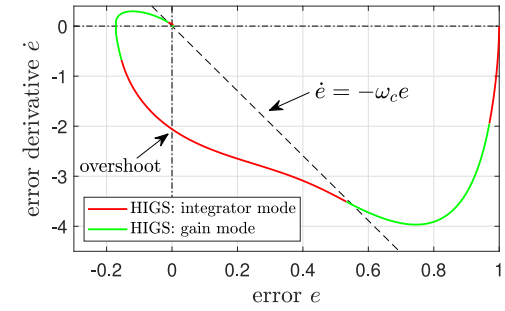

(b) Error e versus error derivative $\dot{e}$ with $\omega_h = 4$ rad/s.

Fig. 6. Trajectories for different values of ω_h.

that multiple zero-crossings of the HIGS' input-output trajectory occur, which is made possible by the specific choice for $\hat{C}_1(s)$, and which result in an oscillatory behaviour around the equilibrium point $(z, u_h) = (0, 0)$.

By construction of z, oscillations around $z = 0$ can be interpreted as oscillations of the $(e, \dot{e})$-trajectory around the line $\dot{e} = -\omega_c e$, as shown in Fig. 5(b). From this figure, a behaviour that somewhat reminds of sliding-mode control is recognized [19]. In a true sliding-mode control set-up, the line $\sigma(\dot{e}, e) = \dot{e} + \omega_c e = 0$, indicated by the dashed black line in Fig. 5(b), can be chosen as the sliding surface, i.e., the invariant manifold to which trajectories converge in finite time. In the HIGS-controlled system, however, the $(\dot{e}, e)$-trajectory does not remain on the line $\sigma = 0$, but rather appears to move in a small neighbourhood of it. Eventually, when the oscillatory behaviour is sufficiently damped out, the trajectory stays close to the line $\sigma = 0$ while operating in gain-mode. The error then approximately evolves by the first-order dynamics $\dot{e} \approx -\omega_c e$.

From the above observations it is apparent that achieving non-overshoot performance relates to the oscillatory nature of the $(e, \dot{e})$-trajectory around the line $\sigma = 0$ as well as the slope of this line. The latter follows from $\omega_c = \omega_h|1 + 4j/\pi|$, and thus depends on ω_h. For $\omega_h \to 0$ the line $\sigma = 0$ tends toward the horizontal line $(e, \dot{e}) = (e, 0)$, whereas for $\omega_h \to \infty$, it tends to the vertical line $(e, \dot{e}) = (0, \dot{e})$. In the former case, oscillatory behaviour around $\sigma = 0$ is permitted, whereas in the latter case no oscillatory behaviour around $\sigma = 0$ can be permitted at all, as this inherently results in overshoot. The $(e, \dot{e})$-trajectories for different values of ω_h are shown in Fig. 6. For small ω_h the behaviour tends to what is expected from chattering around a sliding surface with no overshoot, whereas for larger ω_h, the system overshoots.

The effect of ω_h on overshoot is further portrayed in Fig. 7, which clearly shows a proportional increase of the overshoot for increasing values of ω_h. Essentially, ω_h provides a tuning knob for adjusting the overshoot. This allows for proposing a simple tuning guideline for the HIGS-based controller. First, k_p and ω_i can be obtained by linear design (Section III-A), and ω_h can subsequently be adjusted to tune the level of overshoot, ranging from what is achieved with the LTI controller (8) (for $\omega_h \to \infty$) to no overshoot at all (for $\omega_h < 0.85$).

In a final experiment, robustness of the proposed approach against exogenous disturbances is studied. For this purpose, a disturbance $d = C_l n$ is added to the plant input u, where C_l is a low-pass filter with cut-off frequency at 20 Hz, and

$$P = \begin{bmatrix} 53440.4617 & 18335.7344 & -39.2803 & -631.4622 & 8.5868 & 18022.8392 \\ 18335.7344 & 6305.08284 & -12.5369 & -227.9162 & 3.0039 & 6187.5201 \\ -39.2803 & -12.5369 & 0.0936 & -0.2962 & -0.003318 & -12.9948 \\ -631.4622 & -227.9162 & -0.2962 & 16.572 & -0.143 & -216.0125 \\ 8.5868 & 3.0039 & -0.003318 & -0.143 & 0.004276 & 2.9084 \\ 18022.8392 & 6187.5201 & -12.9948 & -216.0125 & 2.9084 & 6079.2674 \end{bmatrix}, \quad \lambda(P) = \begin{bmatrix} 65819.5072 \\ 21.9178 \\ 0.03129 \\ 0.02267 \\ 0.002330 \\ 0.0006804 \end{bmatrix} \tag{18}$$

$$\Theta = \begin{bmatrix} 300.15307 & 96.0802 & -0.5719 & 2.2052 & -0.02731 & 99.1869 \end{bmatrix} \tag{19}$$

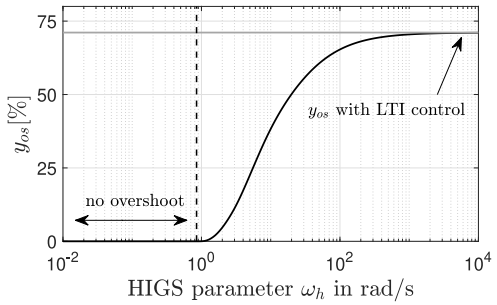

Fig. 7. Percentage of overshoot as a function of ω_h.

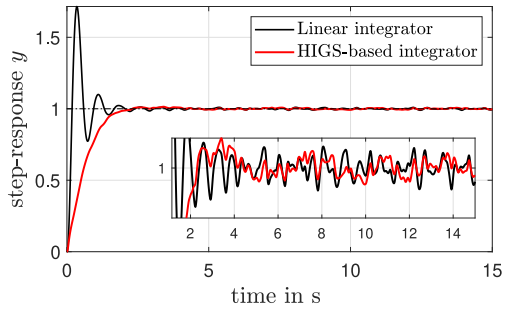

(a) Step-response y when subject to an input disturbance.

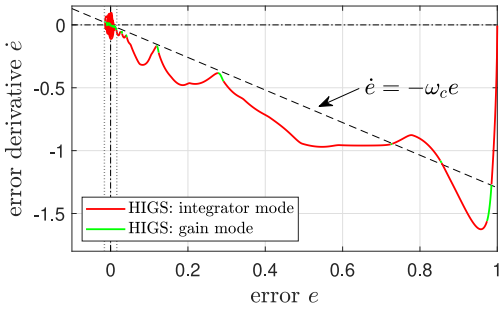

(b) Error e versus error derivative $\dot{e}$ with $\omega_h = 0.8$ rad/s.

Fig. 8. System behaviour when subject to an input disturbance.

n is uniformly distributed zero-mean white-noise, to present, for instance, actuator noise. Simulation results are shown in Fig. 8. It can be seen that overshoot occurs, but remains within a small neighbourhood of the origin determined by the level of disturbance. Note that still the combination of the rise-time and overshoot of the HIGS-controlled system is unattainable by any LTI design. In addition, it can be seen that the $(e, \dot{e})$-trajectory remains close to the line $\sigma = 0$ which suggests that the observed non-overshoot mechanism contributes to the robust performance properties of the proposed approach.

V. Conclusion

In this letter, an example of a HIGS-based controller is discussed that overcomes a fundamental overshoot performance limitation inherent to LTI systems having a real unstable open-loop pole. In particular, a nonlinear integrator is constructed by interconnecting the HIGS in series with specific linear filters. Key in achieving non-overshoot performance is the ordering of the linear filters with respect to HIGS. The insights and established tuning guidelines provide valuable elements for a general control design framework based on HIGS.

Appendix

The matrices (A_1, B_1), (A_2, B_2), and (C, D) of the closed-loop system (13) with input $w = [r, \dot{r}]^\top$, are given in (15), (16), and (17), as shown at the bottom of p. 4, respectively. The parameters are set to $\omega = 5 \cdot 2\pi$ rad/s, $\zeta = 1.5$, $p = 1$, $q = 3$, $k_p = 10$, $\omega_i = 1$ rad/s, $\omega_h = 0.8$ rad/s, $\omega_c = 1.29$ rad/s, and $\tau = 5{\cdot}10^{-3}$. The LMIs in (14) are solved by means of the MATLAB toolbox `Yalmip` [20] together with the external solver `MOSEK` [21]. The matrix P with its corresponding eigenvalues $\lambda(P)$, and the vector θ are given in (18) and (19), respectively, as shown at the bottom of the previous page.

References

[1] R. H. Middleton, "Trade-offs in linear control system design," *Automatica*, vol. 27, no. 2, pp. 281–292, 1991.

[2] M. M. Seron, J. H. Braslavsky, and G. C. Goodwin, *Fundamental Limitations in Filtering and Control*. London, U.K.: Springer-Verlag, 1997.

[3] D. A. Deenen, M. F. Heertjes, W. P. M. H. Heemels, and H. Nijmeijer, "Hybrid integrator design for enhanced tracking in motion control," in *Proc. IEEE Amer. Control Conf. (ACC)*, Seattle, WA, USA, 2017, pp. 2863–2868.

[4] M. F. Heertjes, N. I. Perdiguero, and D. A. Deenen, "Robust control and data-driven tuning of a hybrid integrator-gain system with applications to wafer scanners," *Int. J. Adapt. Control Signal Process.*, vol. 33, no. 2, pp. 371–387, 2018.

[5] J. C. Clegg, "A nonlinear integrator for servomechanisms," *Trans. Amer. Inst. Elect. Eng. II, Appl. Ind.*, vol. 77, no. 1, pp. 41–42, Mar. 1958.

[6] O. Beker, C. V. Hollot, and Y. Chait, "Plant with integrator: An example of reset control overcoming limitations of linear feedback," *IEEE Trans. Autom. Control*, vol. 46, no. 11, pp. 1797–1799, Nov. 2001.

[7] W. H. T. M. Aangenent, G. Witvoet, W. P. M. H. Heemels, M. J. G. van de Molengraft, and M. Steinbuch, "Performance analysis of reset control systems," *Int. J. Robust Nonlin. Control*, vol. 20, no. 11, pp. 1213–1233, 2009.

[8] D. Nesic, A. R. Teel, and L. Zaccarian, "Stability and performance of SISO control systems with first order reset elements," *IEEE Trans. Autom. Control*, vol. 56, no. 11, pp. 2567–2582, Nov. 2011.

[9] S. J. L. M. van Loon, K. G. J. Gruntjens, M. F. Heertjes, N. van de Wouw, and W. P. M. H. Heemels, "Frequency-domain tools for stability analysis of reset control systems," *Automatica*, vol. 82, pp. 101–108, Aug. 2017.

[10] S. J. A. M. van den Eijnden, Y. Knops, and M. F. Heertjes, "A hybrid integrator-gain based low-pass filter for nonlinear motion control," in *Proc. IEEE Conf. Control Technol. Appl. (CCTA)*, Copenhagen, Denmark, 2018, pp. 1108–1113.

[11] G. Zhao, D. Nešić, Y. Tan, and C. Hua, "Overcoming overshoot performance limitations of linear systems with reset control," *Automatica*, vol. 101, pp. 27–35, Mar. 2019.

[12] B. G. B. Hunnekens, N. van de Wouw, and D. Nešić, "Overcoming a fundamental time-domain performance limitation by nonlinear control," *Automatica*, vol. 67, pp. 277–281, May 2016.

[13] B. Sharif, M. F. Heertjes, and W. P. M. H. Heemels, "Extended projected dynamical systems with applications to hybrid integrator-gain systems," in *Proc. IEEE 58th Conf. Decis. Control (CDC)*, Nice, France, 2019, pp. 5773–5778.

[14] R. H. Middleton and G. C. Goodwin, *Digital Control and Estimation. A Unified Approach*. Englewood Cliffs, NJ, USA: Prentice-Hall, 1990.

[15] S. Skogestad and I. Postletwhite, *Multivariable Feedback Control: Analysis and Design*, 2nd ed. Chichester, U.K.: Wiley, 2010.

[16] E. D. Sontag and Y. Wang, "On characterizations of the input-to-state stability property," *Syst. Control Lett.*, vol. 24, no. 5, pp. 351–359, 1995.

[17] G. F. Franklin, J. D. Powell, and A. Emami-Naeini, *Feedback Control of Dynamic Systems*, 5th ed. Upper Saddle River, NJ, USA: Prentice-Hall, 2005.

[18] H. K. Khalil, *Nonlinear Systems*, 3rd ed. Upper Saddle River, NJ, USA: Prentice-Hall, 2002.

[19] C. Edwards and S. K. Spurgeon, *Sliding Mode Control: Theory and Applications*, New York, NY, USA: Taylor & Francis, 1998.

[20] J. Lofberg, "YALMIP: A toolbox for modeling and optimization in MATLAB," in *Proc. IEEE Int. Symp. Comput.-Aided Control Syst. Design*, Taipei, Taiwan, 2004 pp. 285–289.

[21] E. D. Andersen, C. Roos, and T. Terlaky, "On implementing a primal-dual interior-point method for conic quadratic optimization," *Math. Program.*, vol. 95, no. 2, pp. 249–277, 2003.